Journal of Engineering Mathematics **41:** 237–258, 2001.

Numerical investigation of the effect of surfactants on the stability and rheology of emulsions and foam

C. POZRIKIDIS
Department of Mechanical and Aerospace Engineering; University of California, San Diego; La Jolla, California 92093-0411, USA (e-mail: cpozrikidis@ucsd.edu; internet: http://stokes.ucsd.edu/c_pozrikidis)

Received 6 September 2000; accepted in revised form 19 February 2001

Abstract. The simple shear flow of ordered and random, non-dilute and concentrated emulsions resembling foam is considered in the presence of an insoluble surfactant. Numerical investigations conducted by the method of interfacial dynamics for Stokes flow combined with an implicit finite-volume method for computing the evolution of the surfactant concentration illustrate the effect of the surfactant on the rheological properties of the emulsion and on the dynamics and stability of the evolving microstructure. Studies of ordered two-dimensional systems, where the suspended phase is distributed on an evolving doubly-periodic lattice, show that, depending on the capillary number, a surfactant may either destabilize or stabilize a concentrated emulsion by promoting or preventing the rupture of thin films developing between the interfaces of adjacent drops. The capillary number, viscosity ratio, and surfactant diffusivity are found to play an important role in determining the rheological properties of the emulsion and the geometrical properties of the evolving microstructure. Large-scale numerical simulations of random two-dimensional systems with 25 drops suspended in a doubly-periodic flow suggest that the qualitative effect of a surfactant is not altered by strong hydrodynamic interactions associated with intercepting or clustering drops.

Key words: emulsions, interfacial dynamics, surfactants, Stokes flow, suspensions.

1. Introduction

Consider an emulsion consisting of a continous liquid phase and a dispersed liquid or gas phase of a given constitution, and assume that the interfaces are clean and devoid of surfactants and thus exhibit a constant and uniform surface tension γ. When the emulsion undergoes simple shear flow with shear rate k, it exhibits a macroscopic or effective shear viscosity, and develops effective normal stresses and associated normal-stress differences that depend on the reduced shear rate expressed by the capillary number $\mathrm{Ca} \equiv \mu k a/\gamma$; μ is the viscosity of the continuous liquid phase, and a is a characteristic length indicative of the size of the dispersed phase. Because of the ability of the suspended drops or bubbles to deform and thereby accommodate the incident shear flow as well as the perturbation flow generated by their peers, as the capillary number is raised, the effective viscosity is reduced, and the emulsion behaves like a shear-thinning and elastic composite medium.

Introducing a surfactant lowers the surface tension from the value γ_c corresponding to a clean interface to the value γ_0 that is determined by the surfactant concentration and the physical properties of the materials involved. In hydrostatics, surfactants provide short-range repulsion between closely-packed interfaces, and thereby stabilize the interfaces against coalescence, prevent demixing, and allow for long-lived dispersions (*e.g.*, [1]). In hydrodynamics, the presence of a surfactant raises the capillary number above the value computed with respect

to the surface tension of a clean interface, $\mathrm{Ca}_c \equiv \mu k a/\gamma_c$, and thereby tends to lower the effective viscosity of the emulsion.

Now, under the influence of an imposed flow, an insoluble surfactant is convected and diffuses over a stationary or evolving interface to prevent the establishment of strong surfactant concentration gradients. The relative importance of convection and diffusion is determined by the surfactant Péclét number $\mathrm{Pe} = ka^2/D_s$, where D_s is the surfactant surface diffusivity. When the surfactant diffusivity is negligible, whereupon the Péclét number is infinite, the surfactant is convected toward accumulation points until Marangoni tractions due to surface tension gradients immobilize the interface and prevent further convective action, allowing for a steady surfactant concentration distribution to be established at equilibrium.

In the limit of small shear rates or vanishing capillary number, the surfactant concentration distribution is nearly uniform, and the effective rheological properties of an emulsion may be deduced from those in the absence of surfactants; the correspondence is made for $\mathrm{Ca}_0 = \mathrm{Ca}$, where $\mathrm{Ca}_0 \equiv \mu k a/\gamma_0$ is the capillary number defined with respect to the surface tension of an interface with a uniform distribution of surfactants and associated uniform surface tension γ_0. At higher shear rates, the analogy breaks down for two reasons. First, surfactant dilusion due to interface stretching raises the surface tension toward the value γ_c corresponding to a clean interface, and thereby lowers the capillary number and tends to increase the effective viscosity of the emulsion. Second, the establishment of surfactant concentration gradients and accompanied variations in surface tension generate Marangoni tractions that partially immobilize portions of the interfaces, and thereby also raise the effective viscosity of the emulsion. Thus, adding a surfactant may, in fact, cause an overall increase in the effective viscosity of the emulsion with respect to the value observed in its absence.

The potentially subtle effect of surfactants on the rheology of emulsions has motivated a detailed investigation of the individual or combined effects of (a) the sensitivity of the surface tension to the surfactant concentration, known as the surface elasticity, (b) the surfactant diffusivity expressed by the surfactant Péclét number, (c) and the capillary number expressing the strength of the flow. Previous authors have studied these dependencies for infinitely dilute systems where hydrodynamic interactions are negligible and the suspended bubbles or drops may be studied in isolation [2, 3]. Our first goal in this work is to extend the previous results to nondilute systems by considering ordered and random systems at non-infinitesimal volume fractions.

Apart from their significance on rheology, surfactants also affect the stability of the dispersed phase, especially when the viscosity of the dispersed drops is significantly lower than that of the continuous phase, and in the limit of high volume fractions. Under these conditions, a concentrated emulsion reduces to a wet foam, and the hydrodynamics is dominated by thin-film flows occurring between adjacent interfaces. Now, because of variations in surface tension due to surfactant concentration gradients, certain portions of the interfaces are more deformable than others, and thus more susceptible to the deforming action of the imposed flow. The increased deformability may potentially lead to interface coalescence and film breakup in the absence of a stabilizing action. Thus, while introducing a surfactant may be beneficial on the rheological properties, it may nevertheless affect the stability of the dispersion in an adverse way. Our second goal in this work is to explicitly demonstrate that surfactants may either promote or undermine the stability of a concentrated emulsion resembling a foam.

As the volume fraction of the suspended phase tends to unity, a wet foam reduces to a dry foam consisting of ordered or random arrangements of gas bubbles separated by thin films that contain a negligible amount of liquid. The statics and rheology of dry foam have been studied

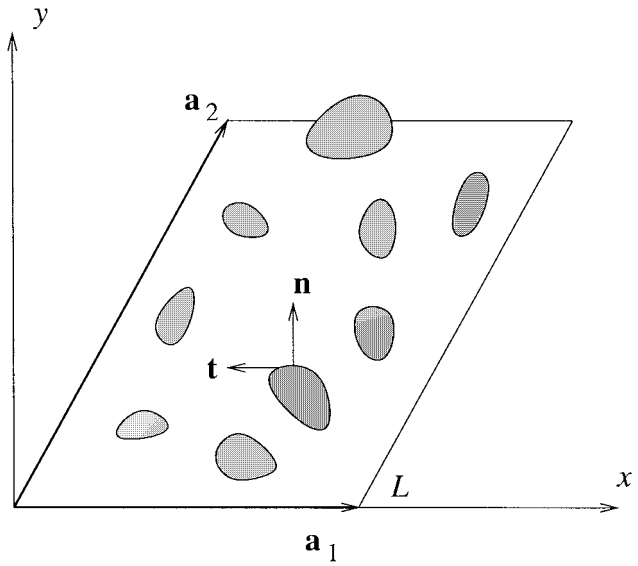

Figure 1. A two-dimensional, doubly-periodic, polydisperse emulsion in the xy plane consisting of a continuous liquid phase and a dispersed gaseous or liquid phase, undergoing simple shear flow.

extensively by previous authors, as reviewed by Reinelt and Kraynik [4]. The present work addresses a complementary set of conditions where fluid motion plays an important role.

Our investigations rely on numerical studies based on a two-dimensional flow model in which a doubly-periodic emulsion with a specified initial constitution evolves under the action of simple shear flow. The motion of the interfaces is computed by the method of interfacial dynamics for Stokes flow, which involves advancing the position of the interfaces with a velocity that arises by solving an integral equation of the second kind at each time step. The integral representation is simplified by use of the doubly-periodic Green's function of Stokes flow which is available in the form of rapidly converging series. The evolution of the surfactant concentration is computed by solving the convection-diffusion equation over the evolving interfaces using a finite-volume method. In the numerical investigations, we consider ordered systems with a dispersed phase of varying viscosity, and random systems with fluids of equal viscosity. The results illustrate that surface tension variations due to surfactant inhomogeneity affect the behavior of emulsions in several expected or new ways.

2. Flow model and mathematical formulation

Consider an idealized doubly-periodic, polydisperse, two-dimensional emulsion in the xy plane consisting of a continuous liquid phase and a dispersed gaseous or liquid phase, as illustrated in Figure 1. The suspension evolves under the action of a simple shear flow directed along the x axis, where the x component of the velocity varies along the y axis with shear rate k. In the absence of suspended bubbles or drops, the x and y components of the velocity of the homogeneous fluid consisting of the continuous phase alone are given by

$$u_x^\infty = ky, \qquad u_y^\infty = 0. \tag{1}$$

In the presence of suspended drops or bubbles, the periodicity of the emulsion is determined by two evolving base vectors $\mathbf{a}_1$ and $\mathbf{a}_2$, defined such that the velocity and pressure remain

invariant when the origin is shifted by an arbitrary linear combination of these base vectors. The first base vector $\mathbf{a}_1$ with length L points along the x axis and remains constant in time, while the second base vector $\mathbf{a}_2$ is convected as though it were a material vector under the influence of the unperturbed shear flow expressed by (1).

Each flow cell contains N bubbles or drops with generally different viscosities μ_i, $i = 1, \ldots N$, suspended in an ambient liquid with viscosity μ_c, where the subscript c denotes the continuous phase. The interface between the ith bubble or drop and the suspending fluid exhibits surface tension γ that is allowed to vary over the interfaces due to the presence of an insoluble surfactant.

The Reynolds number of the flow in the continuous phase and inside the drops is assumed to be so small that the effect of fuid inertia is negligible, and the motion of the fluid is governed by the linear equations of Stokes flow. Moreover, gravitational forces are assumed negligible, and the drops are effectively neutrally buoyant. Subject to these assumptions, the velocity $\mathbf{u}$ and pressure p in the continuous phase satisfy the continuity equation and the homogeneous Stokes equation

$$\nabla \cdot \mathbf{u} = 0, \qquad \nabla p = \mu_c \, \nabla^2 \mathbf{u}. \tag{1}$$

The flow inside the ith drop is governed by the corresponding equations

$$\nabla \cdot \mathbf{u} = 0, \qquad \nabla p = \mu_i \, \nabla^2 \mathbf{u}, \tag{2}$$

where $i = 1, \ldots N$.

The velocity is required to be continuous across the interfaces, but the hydrodynamic traction $\mathbf{f} = \sigma \cdot \mathbf{n}$ undergoes a discontinuity determined by the surface tension; σ is the Newtonian stress tensor, and $\mathbf{n}$ is the unit vector normal to an interface pointing into the ambient fluid. An interfacial force balance shows that the traction discontinuity across the mth interface is given by

$$\Delta \mathbf{f} \equiv \mathbf{f}^{(c)} - \mathbf{f}^{(m)} = (\sigma^{(c)} - \sigma^{(m)}) \cdot \mathbf{n} = -\frac{\partial(\gamma \mathbf{t})}{\partial l} = \kappa \, \gamma \, \mathbf{n} - \frac{\partial \gamma}{\partial l} \, \mathbf{t}, \tag{3}$$

where $\kappa = \nabla \cdot \mathbf{n}$ is the curvature of the interface in the xy plane, l is the arc length along the interface measured from an arbitrary origin in the direction of the unit tangent vector $\mathbf{t}$, the superscript (c) denotes that the underlying variable is evaluate on the side of the continuous phase, and the superscript (m) denotes that the underlying variable is evaluated on the side of the mth drop or bubble.

An insoluble surfactant is present at each interface, and is both convected by the interfacial velocity field and diffuses over the interface but not off the interface into the suspending or suspended phase. The surfactant concentration Γ over the mth interface changes according to the evolution equation

$$\frac{\mathrm{D}\Gamma}{\mathrm{D}t} = -\Gamma \, \frac{\partial(\mathbf{u} \cdot \mathbf{t})}{\partial l} - \Gamma \kappa \, \mathbf{u} \cdot \mathbf{n} + D_s \frac{\partial^2 \Gamma}{\partial l^2}, \tag{4}$$

where $\mathrm{D}/\mathrm{D}t$ is the material derivative, and D_s is the surfactant diffusivity. The first and second terms on the right-hand side of (4) express, respectively, changes in the surfactant concentration due to interface stretching or expansion.

We shall assume that the surface tension is related to the surfactant concentration by the linear equation of state

$$\gamma = \frac{\gamma_0}{1-\beta}\left(1-\beta\frac{\Gamma}{\Gamma_0}\right), \tag{5}$$

where β is a positive physicochemical constant expressing the sensitivity of the surface tension to the surfactant concentration, and γ_0 is the surface tension corresponding to the reference surfactant concentration Γ_0. The physical limitations of this linear relationship, which is accurate only for small variations in the surfactant concentration, are discussed by Johnson and Borhan [5].

The effective rheological properties of the emulsion are expressed by the effective stress tensor σ^{Eff}, defined as the areal average of the stress tensor over one period of the flow. Using integral identities, we find that the effective stress tensor may be expressed in terms of line integrals along the interfaces involving the jump in the interfacial traction and the interfacial velocity, in the form

$$\begin{aligned}\sigma_{ij}^{\text{Eff}} = & -\delta_{ij}\,\langle p\rangle + 2\,\mu_c\langle e_{ij}\rangle \\ & + \frac{1}{A_c}\sum_{m=1}^{N}\int_{C_m}[\Delta f_i\, x_j - \mu_c\,(1-\lambda_m)(u_i n_j + u_j n_i)]\,\mathrm{d}l,\end{aligned} \tag{6}$$

where the pointed brackets denote the areal average, e_{ij} is the rate-of-deformation tensor, C_m is the interface of the mth drop, $A_c = |\mathbf{a}_1 \times \mathbf{a}_2|$ is the area of each periodic flow cell, and $\lambda_m \equiv \mu_m/\mu_c$ is the viscosity ratio of the mth drop. The last term on the right-hand side of (6), involving the sum, expresses the contribution of the suspended phase.

Considering the first term of the integrand in (6), we use Equation (3) and integrate by parts to write

$$\int_{C_m}\Delta f_i\, x_j\,\mathrm{d}l = \int_{C_m}\gamma t_i t_j\,\mathrm{d}l = \int_{C_m}\gamma\,(\delta_{ij}-n_i n_j)\,\mathrm{d}l, \tag{7}$$

where $\mathbf{t}$ is the unit vector tangent to the interface, and the surface tension is allowed to be a function of position over the interface. Expression (6) allows us to compute the effective stresses from knowledge of the interfacial distribution of the surface tension and velocity, where the former is determined by the instantaneous surfactant distribution. When all viscosity ratios are equal to unity, the distribution of the interfacial velocity is not required. Equation (6) and the expression on the right-hand side of (7) are also applicable to three-dimensional flow, provided that the integral with respect to arc length is replaced by a surface integral, and A_c is replaced by the volume of a three-dimensional unit cell [4, 6].

The rheological properties of the emulsion under consideration are expressed by the effective shear viscosity defined as $\mu_{\text{Eff}} \equiv \sigma_{xy}^{\text{Eff}}/k$, and the effective normal stress difference defined as $N_{\text{Eff}} \equiv \sigma_{xx} - \sigma_{yy}$. The dimensionless effective viscosity and normal stress difference are defined as $\hat{\mu}_{\text{Eff}} \equiv \mu_{\text{Eff}}/\mu_c$ and $\hat{N}_{\text{Eff}} \equiv N_{\text{Eff}}/(k\mu_c)$.

Consider, for illustration, a laminated suspension consisting of N infinite bands oriented along the x axis with uniform concentration of surfactants, and regard each period of a band as a drop. Because the interfaces are flat, the jump in traction vanishes, and the integral after the sum in (6) reduces to

$$\int_{C_m}(\mu_m-\mu_c)(u_i n_j + u_j n_i)\,\mathrm{d}l = k(1-\delta_{ij})(\mu_m-\mu_c)A_m, \tag{8}$$

where A_m is the area occupied by the mth band. Substituting this expression in (6), we find that the effective viscosity of the laminated fluid is equal to the weighted areal average of the viscosity of the individual fluids, as expected.

In the case of a highly concentrated emulsion resembling a foam, adjacent interfaces belonging to different drops or bubbles are nearly parallel everywhere except at the Plateau borders where the thin films meet at multiple junctions. In the absence of motion, or when the foam is dry, the effective stress tensor is given by the simplified version of (6)

$$\sigma_{ij}^{\text{Eff}} = -\delta_{ij}\,\langle p\rangle + \frac{1}{A_c}\sum_{m=1}^{N}\int_{C_m}\gamma t_i t_j\,\mathrm{d}l. \tag{9}$$

When the surface tension is uniform, the effective pressure of the two-dimensional emulsion is given by

$$p_{\text{Eff}} \equiv -\frac{1}{2}\text{Trace}(\sigma^{\text{Eff}}) = \langle p\rangle - \frac{\gamma}{2A_c}\sum_{m=1}^{N} L_m, \tag{10}$$

where L_m is the length of the mth interface. The first term on the right-hand side of (10) is the area-averaged pressure over one period of the emulsion. Rearranging (10), we obtain an equation of state for a stationary or dry foam,

$$p_{\text{Eff}}A_c + \frac{\gamma}{2}\sum_{m=1}^{N} L_m = \langle p\rangle A_c, \tag{11}$$

derived by previous authors on the basis of energetics or using the principle of virtual displacements [7]. The counterpart of (11) for a three-dimensional foam is

$$p_{\text{Eff}}V_c + \frac{2\gamma}{3}\sum_{m=1}^{N} S_m = \langle p\rangle V_c, \tag{12}$$

where V_c is the volume of a cell, and S_m is the surface area of the mth interface [7].

3. Integral representation and numerical method

To compute the evolution of the interfaces, we use the boundary integral formulation for two-dimensional Stokes flow involving the doubly-periodic Green's function (*e.g.*, [8]). Choosing as control volume one periodic flow cell, and exploiting the periodicity of the velocity and pressure and the conforming periodicity of the Green's function to discard integrals over periodic segments confining the control volume, we find that the velocity at a point $\mathbf{x}_0$ located in the suspending phase is given by the integral representation

$$\begin{aligned} u_j(\mathbf{x}_0) = {} & u_j^{\infty}(\mathbf{x}_0) - \frac{1}{4\pi\mu_c}\sum_{m=1}^{N}\int_{C_m}\Delta f_i(\mathbf{x})G_{ij}^{2D-2P}(\mathbf{x},\mathbf{x}_0)\mathrm{d}l(\mathbf{x}) \\ & + \frac{1}{4\pi}\sum_{m=1}^{N}(1-\lambda_m)\int_{C_m} u_i(\mathbf{x})T_{ijk}^{2D-2P}(\mathbf{x},\mathbf{x}_0)n_k(\mathbf{x})\mathrm{d}l(\mathbf{x}), \end{aligned} \tag{13}$$

where $\mathbf{u}^{\infty}$ is the unperturbed flow given in (1). The kernels $G_{ij}^{2D-2P}(\mathbf{x}, \mathbf{x}_0)$ and $T_{ijk}^{1P-W}(\mathbf{x}, \mathbf{x}_0)$ of the single- and double-layer potential on the right-hand side of (9) are the doubly-periodic Green's functions of two-dimensional Stokes flow representing the velocity and stress at the point $\mathbf{x}$ due to a lattice of point forces whose geometry corresponds to the instantaneous structure of the doubly-periodic emulsion; one of the point forces is located at the evaluation point $\mathbf{x}_0$. Expressions for the Green's functions in terms of rapidly converging Ewald sums have been derived by van de Vorst [9] and are presented in adapted form that is consistent with the present notation at the Appendix. Periodic Green's functions of the equations of Stokes flow, Laplace's equation, and Helmholtz's equation have been derived, discussed, and used in boundary-integral formulations by several previous authors [10–17].

The velocity at a point $\mathbf{x}_0$ located inside the qth drop is given by the representation (9), except that all terms on the right-hand side are divided by the viscosity ratio λ_q. Taking the limit as the point $\mathbf{x}_0$ approaches the interface of the qth drop from the interior or exterior side, and expressing the limit of the double-layer potential in terms of the principal value, we obtain a system of integral equations for the velocity at the interfaces. For a point $\mathbf{x}_0$ located at the interface of the qth drop, the integral equation reads

$$u_j(\mathbf{x}_0) = \frac{2}{1+\lambda_q}\left[u_j^{\infty}(\mathbf{x}_0) - \frac{1}{4\pi\mu_c}\sum_{m=1}^{N}\int_{C_m}\Delta f_i(\mathbf{x})G_{ij}^{2D-2P}(\mathbf{x},\mathbf{x}_0)\mathrm{d}l(\mathbf{x}) + \frac{1}{4\pi}\sum_{m=1}^{N}(1-\lambda_m)\int_{C_m}^{PV} u_i(\mathbf{x})T_{ijk}^{2D-2P}(\mathbf{x},\mathbf{x}_0)n_k(\mathbf{x})\mathrm{d}l(\mathbf{x})\right], \tag{14}$$

where PV denotes the principal value of the double-layer potential. When all viscosity ratios λ_m are equal, finite, and non-zero, the integral equation (13) is known to have a unique solution that may be computed by the method of successive substitutions. The properties of the integral equation for the more general case of drops with unequal viscosities have not been established.

The integral equation for the interfacial velocity (13), and the convection-diffusion equation for the surfactant concentration (4) were solved using, respectively, a boundary element and an implicit finite-volume method. In the numerical implementation, the integral equation is transformed into a system of linear equations for the velocity at the nodes, and the linear system is solved by Gauss elimination. Time integration was carried out by the second-order Runge–Kutta method with a constant time step.

In the case of ordered emulsions, the Green's function was computed in terms of truncated Ewald sums, as discussed in the Appendix. In the case of random emulsions, the evaluation was done by interpolation through prepared look-up tables with an estimated accuracy of five significant digits. Marker points tracing the interfaces were adaptively redistributed to capture the development of regions of high curvature and to ensure adequate spatial resolution. When new marker points are introduced, the surfactant concentration is computed by fourth-order interpolation with respect to the instantaneous arc length. In the case of ordered emulsions discussed in Section 4, approximately 100 points are distributed along each interface; in the case of random emulsions discussed in Section 5, approximately 30 points are distributed along each one of the 25 interfaces of the dispersed drops.

4. Ordered emulsions

In the first part of the numerical investigation, we consider ordered monodisperse emulsions where each flow cell of area A_c contains one drop of area A_D and equivalent radius $a = \sqrt{A_D/\pi}$. Previous studies have shown that the effect of the surfactant becomes most significant when the viscosity of the dispersed phase is small compared to the viscosity of the continuous phase [2, 3]. Accordingly, in the main body of the numerical studies, we set the drop viscosity equal to 5% of the viscosity of the suspending fluid, corresponding to the viscosity ratio $\lambda = 0{\cdot}05$. Choosing a non-zero value for λ prevents numerical difficulties related to the non-uniqueness of solution of the integral equation due to the implicit constraint of the dispersed phase incompressibility [8].

At the initial instant, the drops are circular, and their centers are located at the vertices of a hexagonal lattice described by the base vectors $\mathbf{a}_1 = (L, 0)$ and $\mathbf{a}_2 = (L/2, \sqrt{3}L/2)$, where L is the distance between two neighboring drop centers, corresponding to the cell area $A_c = \sqrt{3}L^2/2$; consequently, the areal fraction of the suspended phase is $\phi = (a/L)^2\ (2\pi/(\sqrt{3})$. Maximum areal fraction for non-overlapping circular drops occurs when $a = L/2$, and is equal to $\phi_{Max} = 0{\cdot}907$. Nondeforming circular drops moving along the x axis are able to slide over one another as long as a is less than $\sqrt{3}L/4 = 0{\cdot}433L$ corresponding to the critical areal fraction $\phi_{cr} = 0{\cdot}680$, which is pertinent to the limit of vanishing capillary number.

The initial distribution of the surfactant over the circular interfaces is uniform and equal to Γ_0; correspondingly, the initial surface tension is uniform and equal to γ_0. Nondimensionalizing all variables using as time scale the inverse shear rate k^{-1}, length scale the hexagonal lattice side length L, and stress scale μk, we find that the motion of the emulsion is determined by the areal fraction ϕ, the capillary number $\mathrm{Ca}_0 = ka\mu/\gamma_0$ defined with respect to the hydrostatic surface tension, the sensitivity of the surface tension to the surfactant concentration expressed by the dimensionless number β introduced in (5), and the surfactant Péclét number $\mathrm{Pe} = ka^2/D_s$.

In the numerical simulations, each time step was carried out by the second-order Runge-Kutta method requiring approximately 20 sec of CPU time on a 550 MHz Pentium PC running LINUX with the g77 FORTRAN compiler. The area of the drops and the total amount of surfactant are conserved within a less than 0·1% numerical error across the length of a simulation.

Drop interactions in a dilute emulsion at small and moderate areal fractions are weak, and the behavior of the drops is similar to that exhibited by solitary drops suspended in infinite shear flow studied by previous authors [2, 3]. Because of our particular interest in the dynamics of concentration emulsions and foam, in the remainder of this section we focus our attention on an emulsion with initial drop radius $a = 0{\cdot}4545L$ corresponding to the areal fraction $\phi = 0{\cdot}75$, which is larger than the critical areal fraction 0·680 for geometrically permissible motion of non-deformable drops.

4.1. Constant surface tension

To establish a point of reference, we begin by considering the motion in the absence of surfactants where the interfaces have constant and uniform surface tension γ. At small capillary numbers $\mathrm{Ca} \equiv \mu ka/\gamma$, the low deformability of the interfaces prevents overpassing drops from sliding over one another; portions of the interfaces press against one another, and coalescence occurs at a finite time. In the numerical simulations, we observe numerical

oscillations over the upper and lower portions of the interfaces of intercepting drops due to numerical inaccuracies and inadequate spatial resolution. As the capillary number is raised, the interfaces become more deformable, and a time-periodic motion with period equal to the period of recurrence of the hexagonal lattice, $T = 2k^{-1}/\sqrt{3}$, is established.

Figure 2(a-e) depicts instantaneous interfacial profiles at time $t = 3{\cdot}96\, k^{-1}$, for a sequence of decreasing capillary numbers Ca = 0·4545, 0·2273, 0·09090, 0·04545, and 0·030. The dots along the interfaces mark the location of the adaptively distributed interfacial marker points. When Ca = 0·4545, corresponding to Figure 2(a), the drops exhibit significant deformation and the films separating two adjacent drops that belong to the same row thin monotonically in time, as will be discussed in the next paragraph. Lowering the capillary number reduces the extent of the film flow and yields localized interfacial contact, as shown in Figure 2(b). Further reduction in the capillary number allows the establishment of periodic motion where the thickness of the films developing between adjacent drops that belong to the same row, as well as the thickness of the films developing between overpassing drops, oscillate around well-defined mean values, as shown in Figure 2(c). When the capillary number is reduced below a certain threshold, thin films develop between the interfaces of overpassing drops, as shown in Figure 2(d, e). When the capillary number is reduced further, we obtain strong numerical evidence that the interfaces coalesce and the emulsion is destabilized at a finite time, as discussed in the previous paragraph.

The nature of the motion is better illustrated by considering the time evolution of the minimum thickness of the films separating adjacent interfaces, denoted by $h_{\min}$, plotted in Figure 3(a) with respect to dimensionless time $\hat{t} \equiv t/T$ for Ca = 0·4545, 0·2273, 0·09090, 0·04545, and 0·030, where $T = 2k^{-1}/\sqrt{3}$ is the period of recurrence of the hexagonal lattice. The solidity of the lines is proportional to the capillary number; thus, the thickest line corresponds to Ca = 0·4545. All lines, with the exception of the dashed line corresponding to Ca = 0·030, are for the films developing between adjacent drops that belong to the same row; the dashed line corresponds to the strongly fluctuating film developing between overpassing drops. The jumps in the lines for the two highest capillary numbers are due to a sudden shift of the point of minimum film thickness due to interfacial deformation. The results presented in Figure 3(a) show an overall monotonic decay of the minimum film thickness for Ca = 0·4545 and 0·2273, and thus suggest that the emulsion will be destabilized after a long and possibly infinite evolution time, and confirm the establishment of periodic motion for moderate capillary numbers. In reality, monotonically thinning fims are stabilized by interface repulsion due to intermolecular forces arising at sufficiently small thicknesses.

Figure 3(b, c) shows the evolution of the effective viscosity and normal stress difference of the emulsions depicted in Figure 2, for Ca = 0·4545, 0·2273, 0·09090, 0·04545, and 0·030. The solidity of the lines is proportional to the capillary number. All lines originate from the same non-zero and non-unit point corresponding to initially circular drops. The initial effective viscosity has a small positive value, and the initial normal stress difference is zero due to the isotropy of the circular interfaces. In all cases, a nearly periodic evolution with period equal to T is observed at long times. The results shown in Figure 3(b, c) reveal that, as the capillary number is raised, the mean value and the amplitude of fluctuations are both reduced, and the emulsion behaves like a shear-thinning fluid with some elastic properties. The mean value of the relative effective viscosity for Ca = 0·4545 is close to 1·1, which is higher by one order of magnitude than the areal-averaged viscosity of the two fluids; this comparison underlines the significance of the non-unidirectional motion.

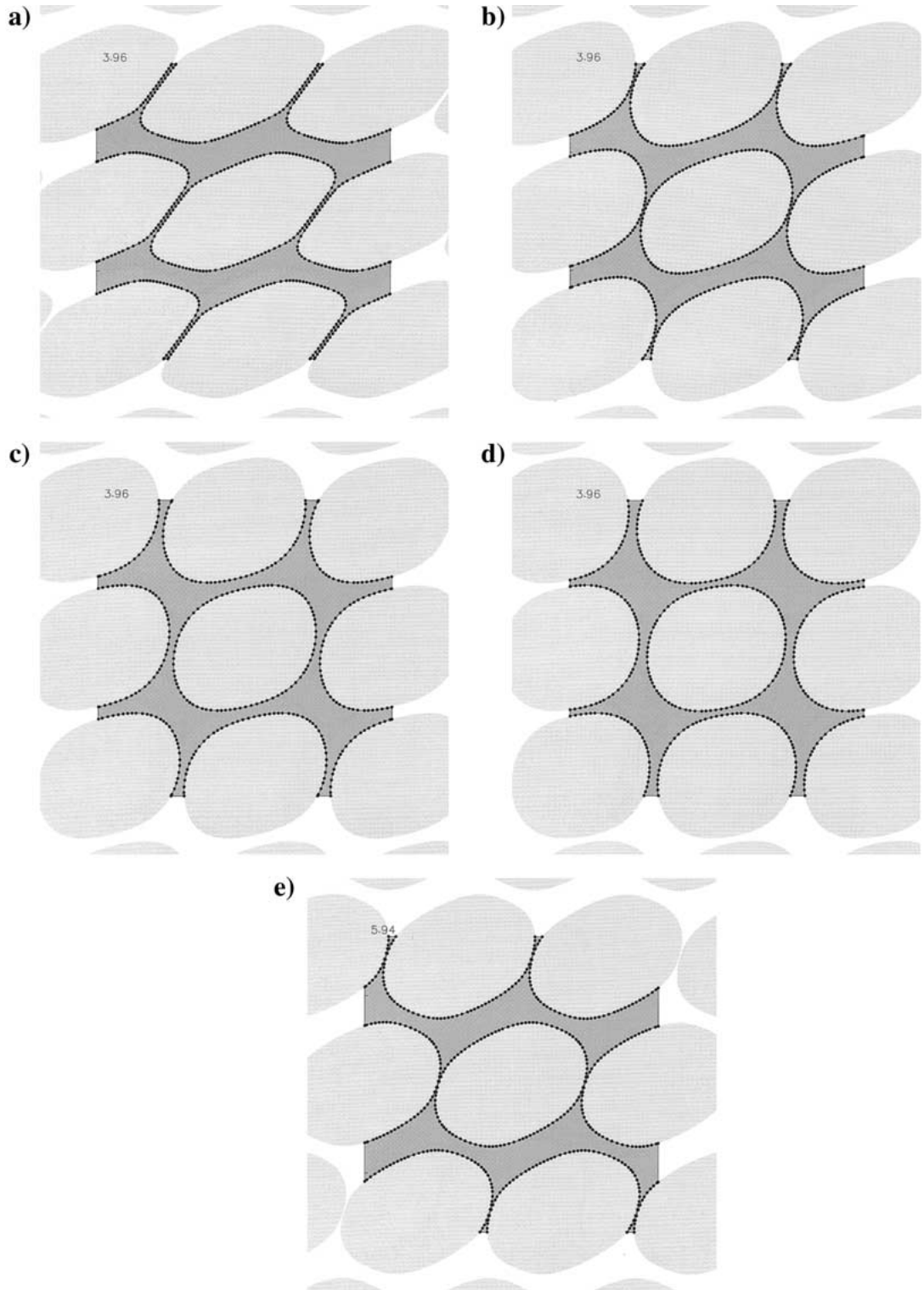

Figure 2. Instantaneous interfacial profiles in an ordered emulsion with a recurrent hexagonal structure in the absence of surfactants, at the areal fraction $\phi = 0{\cdot}75$, at time $t = 3{\cdot}96\, k^{-1}$, for a sequence of decreasing capillary numbers: (a) Ca $= 0{\cdot}4545$, (b) $0{\cdot}2273$, (c) $0{\cdot}09090$, (d) $0{\cdot}04545$, and (e) $0{\cdot}030$.

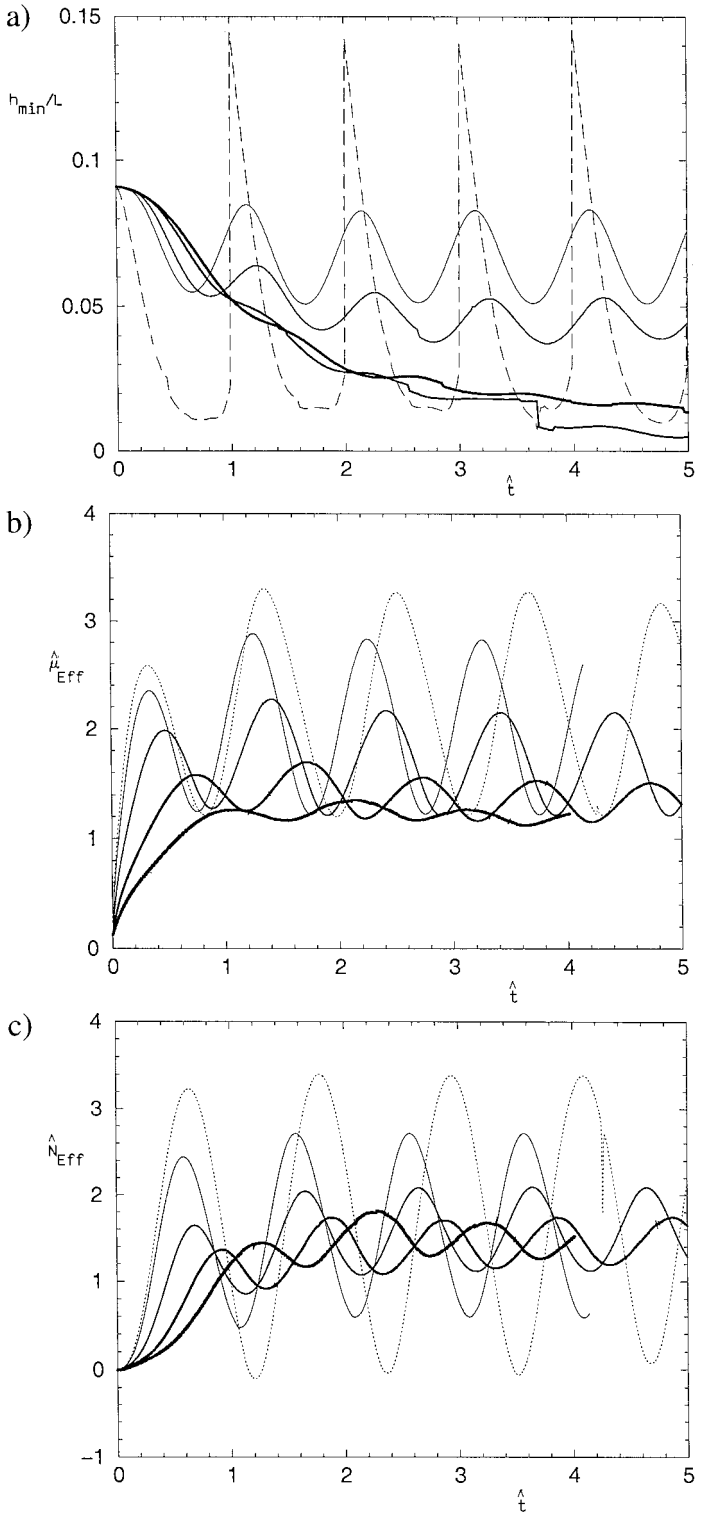

Figure 3. (a) Time evolution of the minimum thickness of the films separating adjacent interfaces for the flows depicted in Figure 2, corresponding to Ca = 0·4545, 0·2273, 0·09090, 0·04545, and 0·030; the solidity of the lines is proportional to the capillary number; all lines, with the exception of the dashed line corresponding to Ca = 0·030, are for the films developing between adjacent drops that belong to the same row. (b, c) Evolution of the effective viscosity and normal stress difference of the suspension; the solidity of the lines is proportional to the capillary number.

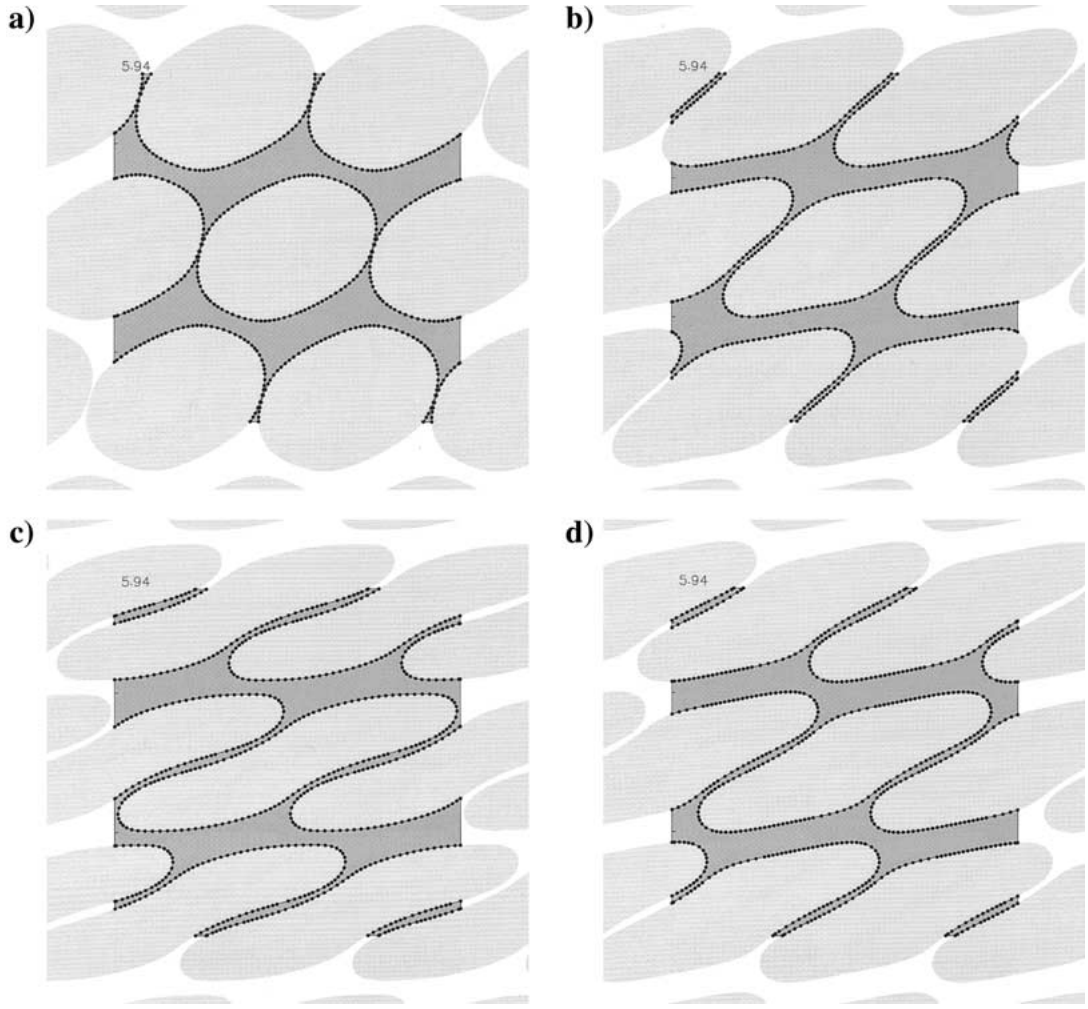

Figure 4. Effect of the viscosity ratio in the absence of surfactants: Instantaneous interface profiles at time $t = 5{\cdot}94\, k^{-1}$, for $\phi = 0{\cdot}75$, Ca $= 0{\cdot}2273$ and (a) $\lambda = 0{\cdot}05$, (b) $1{\cdot}0$, (c) $5{\cdot}0$, and (d) $10{\cdot}0$.

The behavior described earlier in this section for low-viscosity drops with $\lambda = 0{\cdot}05$ resembling incompressible bubbles is qualitatively similar to that reported by Li *et al.* [11] for drops whose viscosity is equal to that of the suspending fluid, corresponding to viscosity ratio λ of unity. To illustrate the effect of the viscosity ratio, in Figure 4(a-d) we display instantaneous interface profiles at time $t = 5{\cdot}94k^{-1}$, for Ca $= 0{\cdot}2273$ and $\lambda = 0{\cdot}05, 1{\cdot}0, 5{\cdot}0,$ and $10{\cdot}0$. The results reveal that raising the viscosity of the drops promotes the deformation of the interfaces, increases the extent of the thin-film-flow between neighboring drops that belong to the same row, and results in sigmoidal and bulbous interfacial shapes. Previous studies have shown that raising the viscosity ratio of solitary drops suspended in infinite shear flow decreases the interface deformation, but also lowers the drop inclination which promotes interactions in a concentrated suspension [18]. These differences underscore the significance of strong hydrodynamic interactions in a concentrated emulsion.

Figure 5(a, b) illustrates the effect of the viscosity ratio on the effective viscosity of the emulsion and on the normal stress difference. The thickness of the lines is proportional to

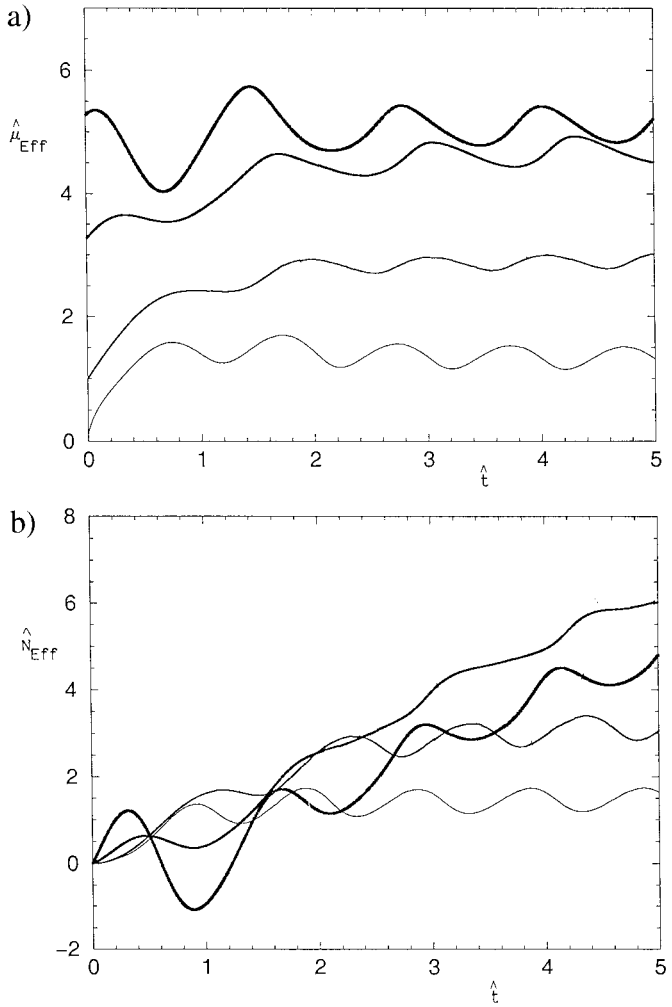

Figure 5. Effect of the viscosity ratio on (a) the effective viscosity, and (b) normal stress difference of the suspension; the thickness of the lines scales with the viscosity ratio.

the viscosity ratio, with the thickest line corresponding to $\lambda = 10$. The mean values of the effective viscosity and normal stress difference are strong functions of the viscosity ratio, but the amplitudes of the fluctuations show a weaker dependence. Figure 5(a) shows that the time scale at which the emulsion approaches a periodic state significantly increases as the viscosity ratio is raised, but the precise effect is hard to quantify.

4.2. Effect of surfactants

Next, we investigate the effect of a surfactant with reference to the motion under constant surface tension illustrated in Figure 2 for $\lambda = 0{\cdot}05$. Figure 6(a, b) shows instantaneous interface profiles after evolution time $t = 3{\cdot}96k^{-1}$ for capillary number $\mathrm{Ca}_0 = 0{\cdot}04545$, where $\mathrm{Ca}_0 \equiv \mu ka/\gamma_0$ is defined with respect to the surface tension of the initially circular undeformed interfaces, γ_0. The corresponding profiles for constant surface tension at the same capillary number are shown in Figure 2(d). Figure 6(a) corresponds to $\beta = 0{\cdot}50$ and $\mathrm{Pe} = 1{\cdot}0$ where surfactant convection is comparable to diffusion, and Figure 6(b) corresponds

to $\beta = 0{\cdot}50$ and $\mathrm{Pe} = 10{\cdot}0$ where surfactant convection dominates diffusion. A comparison of the three profiles reveals that the presence of a weakly diffusing surfactant reduces the film thickness of adjacent drops, and thereby destabilizes the motion of a concentrated emulsion.

The mechanism by which this occurs becomes evident by inspecting the distribution of the surfactant concentration over the interfaces plotted in Figure 6(c) with respect to the polar angle θ measured the around center of a drop. The dashed line corresponds to $\mathrm{Pe} = 1$, and the dotted line corresponds to $\mathrm{Pe} = 10$. The graphs reveal increased surfactant concentration over the northeastern and southwestern portion of each interface, and reduced surfactant concentration over the upper and lower side of each drop. The synergistic effect promotes the overall drop deformation, causes a significant reduction in the film thickness between two drops that belong to the same row, and tends to destabilize the emulsion.

When significant surfactant concentration and associated surface tension gradients have been established, portions of the interfaces are partially immobilized due to the onset of Marangoni tractions. Figure 6(d) shows the distribution of the tangential velocity over an interface corresponding to the profiles shown in Figures 2(d) and 6(a, b) drawn, respectively, with the solid, dashed, and dotted line. A significant reduction in the magnitude of the tangential velocity over the upper and lower portion of the interfaces is evident in the third case. If the interfaces were completely immobilized, the drops would translate like arrays of rigid bodies with strong lubrication forces developing between adjacent rows, and this would drastically increase the effective rheological properties of the emulsion.

Figure 7(a) shows the time evolution of the minimum film thickness; the solid line corresponds to constant surface tension, the dashed line corresponds to $\beta = 0{\cdot}50$ and $\mathrm{Pe} = 1{\cdot}0$, and the dotted line corresponds to $\beta = 0{\cdot}50$ and $\mathrm{Pe} = 10{\cdot}0$. In spite of significant numerical noise, it is evident that, in the third case, the minimum film thickness decreases monotonically in time destabilizing the emulsion.

The presence of surfactants has a strong effect on the rheological properties of the emulsion. Figure 7(b, c) shows the evolution of the effective viscosity and normal stress difference plotted with respect to reduced time $\hat{t} = t/T$. The mean values for $\beta = 0{\cdot}50$ and $\mathrm{Pe} = 10{\cdot}0$ are higher that those for constant surface tension nearly by a factor of three due to the establishment of significant Marangoni tractions. An analogous increase in the rheological properties of a infinitely dilute emulsion of three-dimensional low-viscosity drops was reported previously by Yon and Pozrikidis [3]. The present results show that the effect is much more pronounced at non-infinitesimal volume fractions due to strong hydrodynamic interactions.

Further numerical simulations have shown that similar effects arise at higher capillary numbers. Figure 8(a) shows instantaneous interface profiles at the higher capillary number $\mathrm{Ca}_0 = 0{\cdot}4545$ for $\beta = 0{\cdot}5$ and $\mathrm{Pe} = 1{\cdot}0$; the corresponding profiles for constant surface tension are shown in Figure 2(a). Comparing the two figures, we find that the presence of a surfactant promotes the extent of the thin-film flow between adjacent interfaces, and causes the formation of more slender diamond-shaped shapes. Figure 8(b) shows the distribution of the surfactant concentration along one of the interfaces depicted in Figure 8(a), plotted with respect to the polar angle measured around the center of a drop. The results reveal the establishment of significant concentration gradients and associated Marangoni tractions.

Simulations at low capillary numbers showed that the accumulation of surfactant at the northeastern and southwestern portions of the interfaces, and associated reduction in surface tension, promotes the local deformability of the drops and allows overpassing drops to accomodate one another with greater ease than in the case of constant surface tension. Thus,

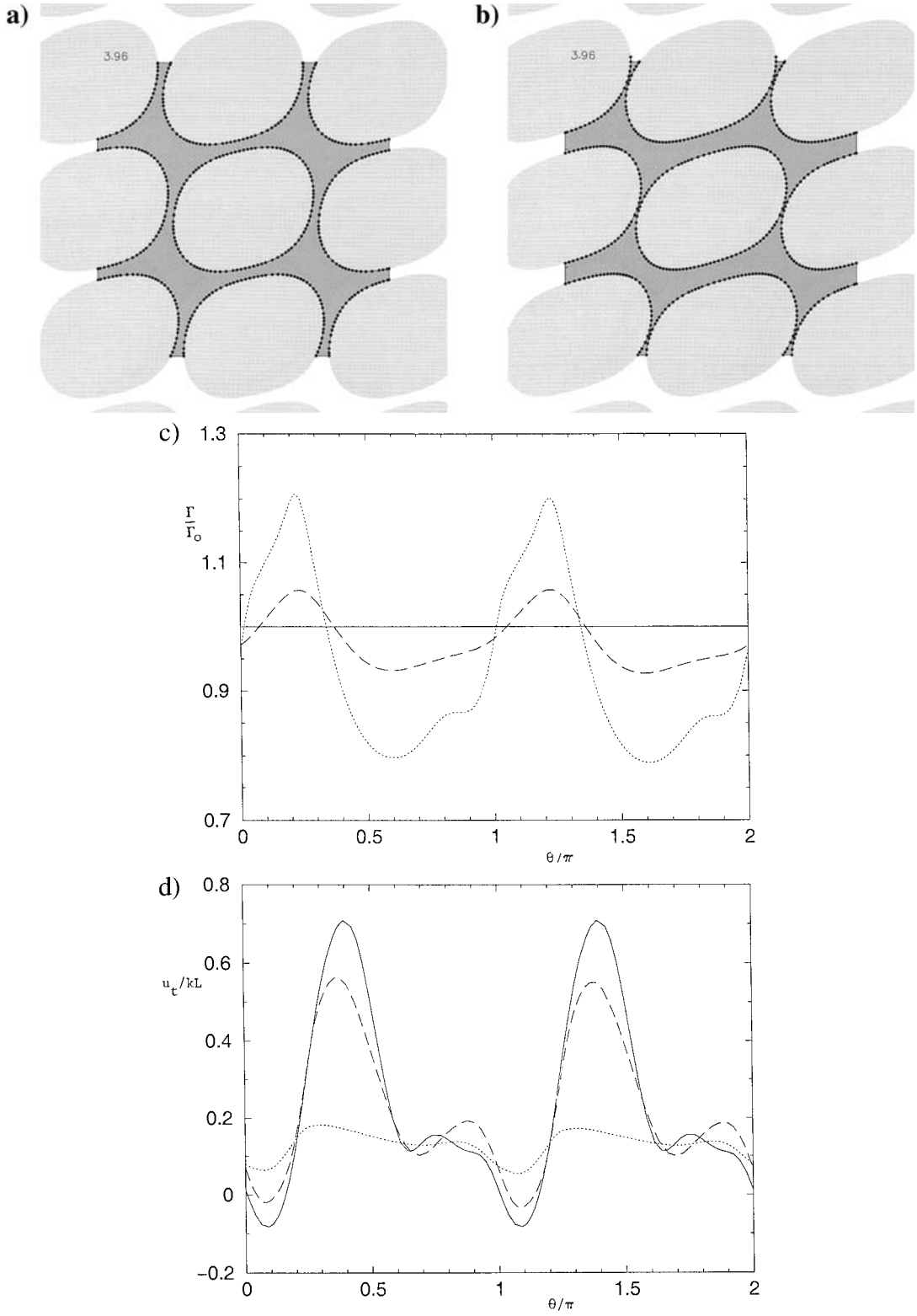

Figure 6. Effect of surfactants: Instantaneous interfacial profiles after evolution time $t = 3{\cdot}96\ k^{-1}$, for capillary number $\mathrm{Ca}_0 = 0{\cdot}04545$, and (a) $\beta = 0{\cdot}50$ and $\mathrm{Pe} = 1{\cdot}0$, or (b) $\beta = 0{\cdot}50$ and $\mathrm{Pe} = 10{\cdot}0$. Interfacial distribution of (d) the surfactant concentration, and (e) tangential velocity along the interfaces shown in (a) and (b).

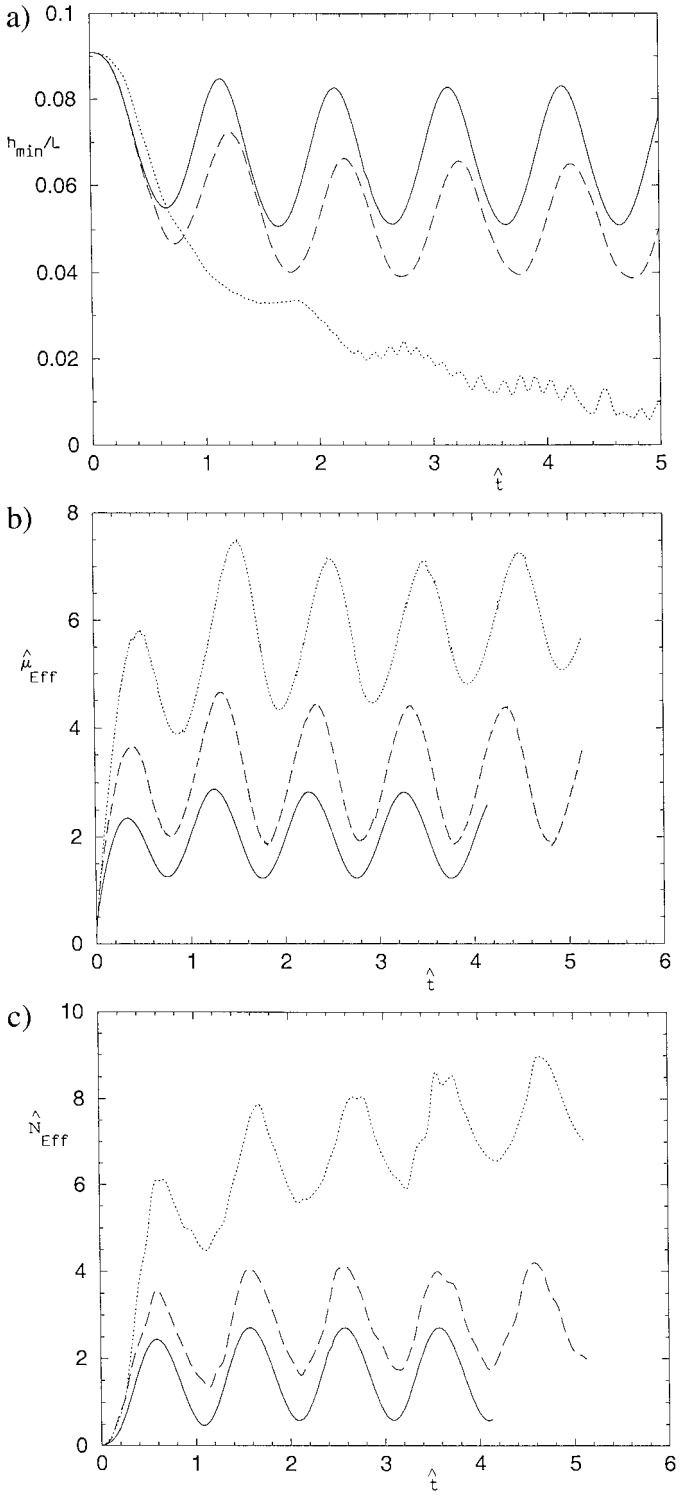

Figure 7. Evolution of (a) the minimum film thickness, and (b, c) effective rheological properties corresponding to the motion illustrated in Figure 6. The solid lines are for constant surface tension, the dashed lines are for $\mathrm{Pe} = 1{\cdot}0$, and the dotted lines are for $\mathrm{Pe} = 10{\cdot}0$.

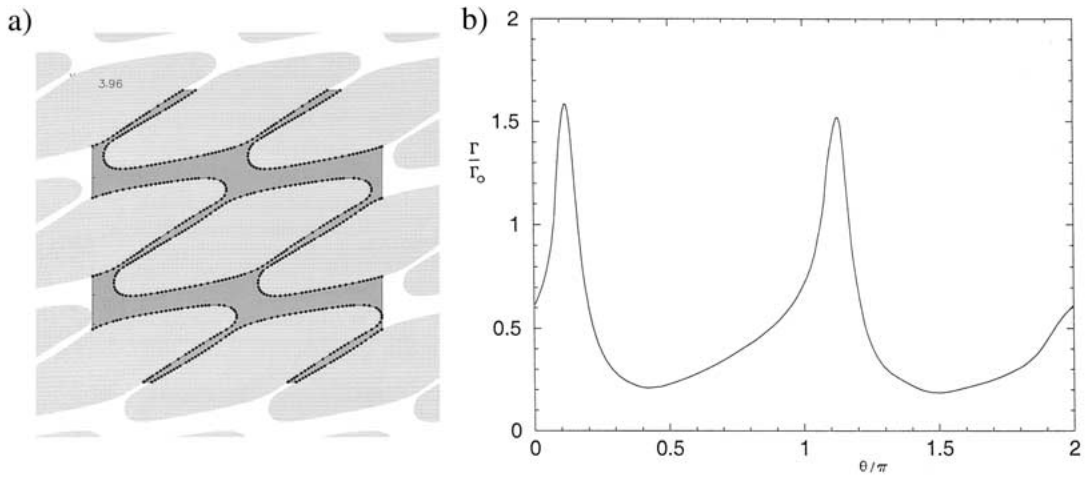

Figure 8. (a) Instantaneous interfacial profiles for $Ca_0 = 0{\cdot}4545$, $\beta = 0{\cdot}5$ and $Pe = 1{\cdot}0$; (b) associated distribution of the surfactant concentration.

the presence of a surfactant promotes the stability of the evolving hexagonal lattice at low capillary numbers.

5. Random emulsions

In the second part of the numerical investigation, we consider the shear flow of random systems with the main goal of studying the effect of a surfactant on the effective rheological properties of the emulsion. At the initial instant, N identical circular drops of radius a are distributed randomly inside a doubly-periodic square computational box of side length L and cell area $A_c = L^2$, and the motion of the interfaces and evolution of the surfactant concentration are computed using the numerical methods discussed in Section 3. Because of subtleties in, and high computational cost required for solving integral equation for the interfacial velocity [19, 20], only monodisperse systems with all viscosity ratios equal to unity were considered, corresponding to viscosity ratios $\lambda_m = 1$ for $m = 1, \ldots N$. Unfortunately, when the viscosity of the suspended phase is comparable to, or greater than, the viscosity of the suspending liquid, the effect of the surfactant is small. The significance of the present simulations then lies in illustrating the qualitative effect of the surfactant, with the expectation that a similar but more pronounced effect will be observed when the viscosity of the suspended phase is small. Previous simulations for infinite dilute systems corroborate this expectation.

Four extended simulations with $N = 25$ drops suspended in each flow cell were carried out at the low areal fraction $\phi = N\pi a^2/A_c = 0{\cdot}10$ and at the moderate areal fraction $\phi = 0{\cdot}40$, for capillary numbers $Ca = 0{\cdot}15$ or $Ca_0 = 0{\cdot}15$, corresponding, respectively, to clean interfaces and to interfaces occupied by a surfactant. At this moderate capillary number, the interfaces show substantial deformation but do not elongate so much as to develop convoluted shapes that undermine the accuracy of the simulations. In the presence of surfactants, we set $\beta = 0{\cdot}50$ to allow the surfactant to have a singificant influence, and $Pe = 1{\cdot}0$ to balance diffusion and convection. Higher values of Pe require increased spatial resolution that could not be afforded with the available computational resources. Each simulation requires approximately 8000 time steps, and each time step requires approximately 1 min of CPU time

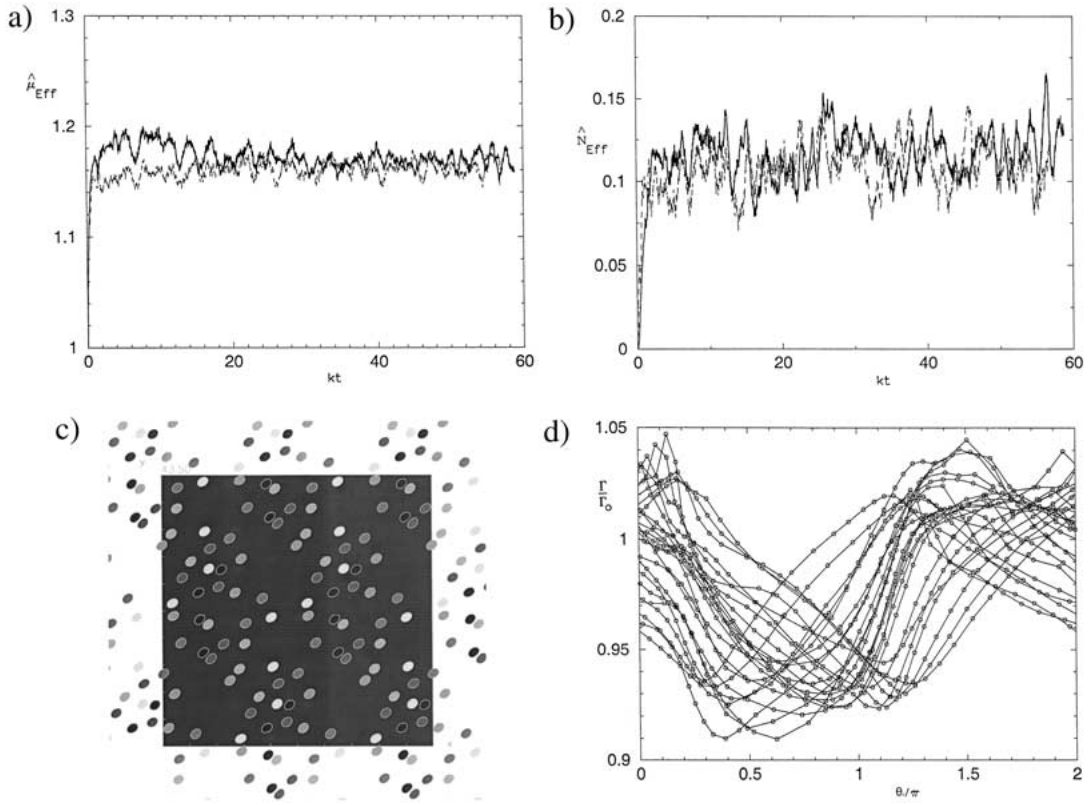

Figure 9. (a, b) Evolution of the reduced effective viscosity and normal stress difference of a dilute suspension with areal fraction $\phi = 0{\cdot}10$. The thin line corresponds to clean interfaces with uniform surface tension, and the heavy line corresponds to interfaces occupied by surfactants. (c) Instantaneous interfacial profiles, and (d) associated distribution of the surfactant concentration.

on the computational facilities mentioned earlier, for a total cose of one week of CPU time per case study.

Figure 9(a, b) shows the evolution of the reduced effective viscosity and normal stress difference, $\hat{\mu}_{\rm Eff}$ and $\hat{N}_{\rm Eff}$ defined in Section 3, for a dilute suspension with areal fraction $\phi = 0{\cdot}10$. The thin line corresponds to clean interfaces with uniform surface tension, and the heavy line corresponds to interfaces populated by surfactants. Li *et al.* [19] conducted simulations in the absence of surfactants with 49 drops suspended in each unit cell using a different implementation of the numerical method, and reported the mean values $\hat{\mu}_{\rm Eff} = 1{\cdot}16$ and $\hat{N}_{\rm Eff} = 0{\cdot}11$, which are in excellent agreement with those deduced from the graphs shown in Figure 9(a, b).

Comparing the two recordings in Figure 9(a, b), we find that the presence of a surfactant raises the mean values and the amplitude of the fluctuations of the effective viscosity and normal stress difference; this is attributed to a decrease in the effective capillary number caused by surfactant dilusion and to the onset of Marangoni tractions. A similar small effect was reported previously for three-dimensional solitary drops corresponding to infinitely dilute emulsions [2, 3]. Figure 9(c) shows an instantaneous snapshot of the computed interfacial profiles in the presence of surfactants, illustrating occasional pairwise drop interceptions, and Figure 9(d) shows the associated distribution of the surfactant concentration over all 25 interfaces plotted

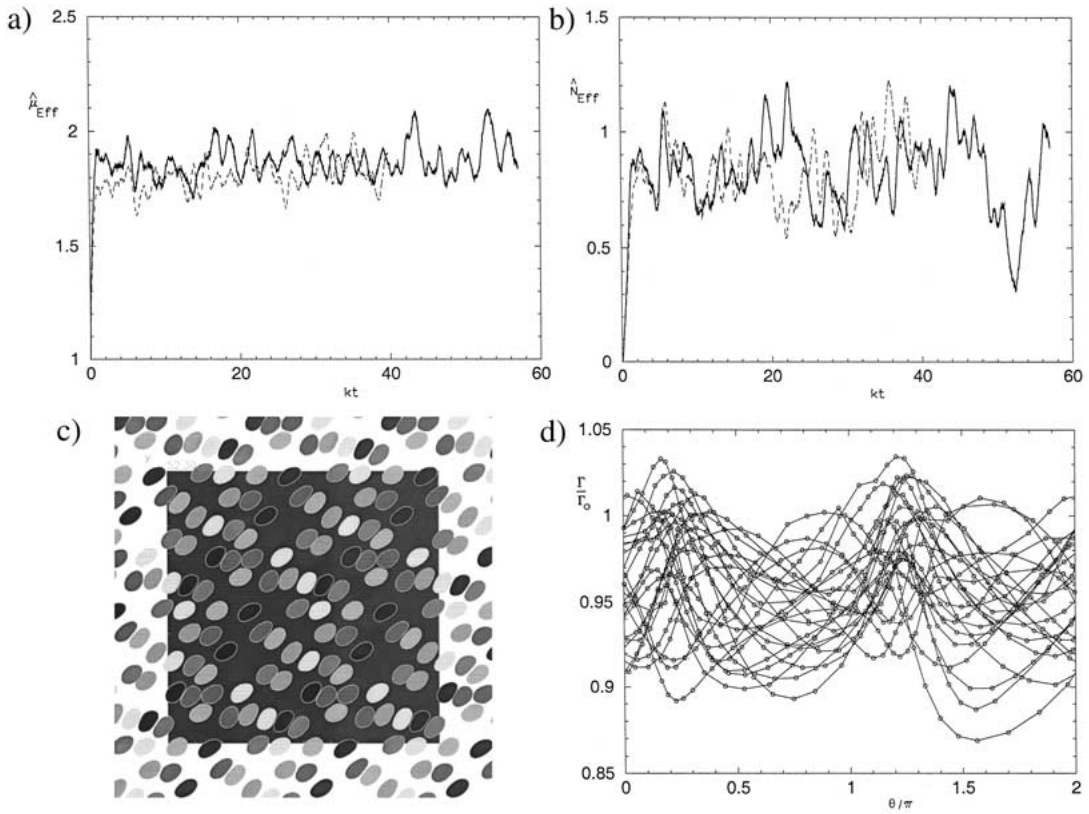

Figure 10. Same as Figure 9 but for the higher areal fraction $\phi = 0{\cdot}40$.

with respect to the polar angle measured around the center of each drop. The variation in the surfactant concentration is approximately 15 % the initial uniform value. The corresponding variation in the surface tension spans a comparable range.

Figure 10(a, b) shows the evolution of the reduced effective viscosity and normal stress difference for a more concentrated suspension at the areal fraction $\phi = 0{\cdot}40$. The thin line corresponds to uniform surface tension, and the heavy line corresponds to interfaces populated by surfactants. Li *et al.* [19] conducted simulations with 49 drops in the absence of surfactants, and reported the mean values $\hat{\mu}_{\mathrm{Eff}} = 1{\cdot}84$ and $\hat{N}_{\mathrm{Eff}} = 0{\cdot}86$, which are in excellent agreement with the mean values deduced from the graphs in Figure 10(a, b). The present of surfactant raises these values only by a small amount. Thus, strong hydrodynamic interactions and multiple drop interceptions do not alter the qualitative influence of the surfactant. An instantaneous snapshot of the interfacial profiles is shown in Figure 10(c), and the associated distribution of the surfactant concentration over the 25 interfaces is shown in Figure 10(d). The surfactant concentration fluctuates over a range that is comparable to that observed previously at the lower areal fraction. The most noriceable new feature is the large magnitude of the fluctuations in the rheological properties due to strong and multiple drop interactions.

6. Discussion

We have performed dynamical simulations to assess the effect of an insoluble surfactant on the rheology and stability of ordered emulsions, and found that the non-uniform distribution of a surfactant over the interfaces may either destabilize the emulsion or facilitate the motion by allowing overpassing drops to accommodate each other's presence. In the mathematical model, we have neglected repulsive intermolecular forces that stabilize the thin films developing in a highly concentrated emulsion and foam against rupture; thus, destabilization should be interpreted in the limited sense of pure hydrodynamics. In the parametric studies, we have illustrated the effect of the viscosity ratio between the suspended and continuous phase, and found it to have a significant influence on the extent of the thin-film flow.

In the second part of this study, we presented the results of large-scale dynamical simulations of the flow of random emulsions in the presence of a surfactant, considering the case where the viscosity of the suspended phase is equal to the viscosity of the suspending fluid, and found that surfactants raise the effective viscosity and the normal stress differences at low and moderate areal fractions. A similar but stronger effect is expected for emulsions with a low-viscosity suspended-phase; unfortunately, considerations of high computational cost have prevented us from studying such systems. Overall, the present results suggest that strong hydrodynamic interactions at high areal fractions do not alter the qualitative effect of an insoluble surfactant documented in previous studies of dilute suspensions.

Acknowledgements

This research was supported by a grant provided by the National Science Foundation.

Appendix

Consider the flow induced by a doubly-periodic array of two-dimensional point forces in the xy plane located at the vertices of a lattice that is defined by the base vectors $\mathbf{a}^{(1)}$ and $\mathbf{a}^{(2)}$. One of the point forces is located at the point $\mathbf{x}_0 = (x_0, y_0)$, and the nth point force is located at the point $\mathbf{x}_n = (x_n, y_n)$, where $x_n = x_0 + i\, a_x^{(1)} + j\, a_x^{(2)}$, $y_n = y_0 + i\, a_y^{(1)} + j\, a_y^{(2)}$, i and j are two integers, and the index n is defined in terms of the indices i and j using a double-summation formula.

Following the Ewald summation method, we find that the Green's function tensor for the velocity is given by

$$G_{ij}(\mathbf{x}, \mathbf{x}_0) = \sum_n \left\{ \delta_{ij} [\tfrac{1}{2} E(\hat{r}_n^2) - \exp(-\hat{r}_n^2)] + \frac{(x_i - x_{n_i})(x_j - x_{n_j})}{r_n^2} \exp(-\hat{r}_n^2) \right\} + \frac{\pi}{A_c} \sum_m \frac{4 + \hat{k}_m^2}{|\mathbf{k}_m|^2} (\delta_{ij} - \frac{\mathbf{k}_{m_i} \mathbf{k}_{m_j}}{|\mathbf{k}_m|^2}) \cos[\mathbf{k}_m \cdot (\mathbf{x} - \mathbf{x}_0)] \exp(-\frac{\hat{k}_m^2}{4}), \tag{A1}$$

adapted from expression (2.20) of van de Vorst [9]. The first sum on the right-hand side of (A1) with respect to n is over all point forces, and the second sum with respect to m is over the vertices of the reciprocal lattice in wave-number space. The base vectors of the reciprocal lattice are given by

$$\mathbf{b}^{(1)} = \frac{1}{A_c} \mathbf{a}^{(2)} \times \mathbf{e}_z, \qquad \mathbf{b}^{(2)} = \frac{1}{A_c} \mathbf{e}_z \times \mathbf{a}^{(1)}, \tag{A2}$$

where $A_c = |\mathbf{a}^{(1)} \times \mathbf{a}^{(2)}|$ is the area of a unit cell; the vertices of the reciprocal lattice are located at $\mathbf{k}_m = (k_{m_x}, k_{m_y})$, where $k_{m_x} = i\, b_x^{(1)} + j\, b_x^{(2)}$ and $k_{m_y} = i\, b_y^{(1)} + j\, b_y^{(2)}$, i and j are two integers, and the index m is defined in terms of i and j using a double-summation formula; the singular wave number corresponding to $i = 0$ and $j = 0$ is excluded from the second sum in (A1). The rest of the symbols in (A1) are defined as follows: $r_n = \sqrt{(x - x_n)^2 + (y - y_n)^2}$ is the distance of the evaluation point from the nth point force; $\hat{r}_n = \xi\, r_n$ is the reduced dimensionless distance; $\hat{k}_m = \frac{|\mathbf{k}_m|}{\xi}$ is the reduced length of the mth wave numer, E is the exponential integral, and ξ is the Ewald splitting parameter with dimensions of inverse length, determining the balance of the sums in real and reciprocal space. In the limit as ξ tends to zero, we obtain a representation in terms of sums in real space; in the limit as ξ tends to infinity, we obtain a representation in terms of a double Fourier series in reciprocal space. In the numerical computations, the exponential integral is computed using an accurate polynomial approximation.

The corresponding Green's function for the pressure, adapted from expression (2.20) of van de Vorst [9], is

$$\begin{aligned} p_j(\mathbf{x}, \mathbf{x}_0) = \; & \frac{4\pi}{A_c}\,(x_j - x_{0_j}) + 2\sum_n \frac{x_j - x_{n_j}}{r_n^2}\exp(-\hat{r}_n^2) \\ & + \frac{4\pi}{A_c}\sum_m \frac{\mathbf{k}_{m_j}}{|\mathbf{k}_m|^2}\sin[\mathbf{k}_m \cdot (\mathbf{x} - \mathbf{x}_0)]\exp\left(-\frac{\hat{k}_m^2}{4}\right). \end{aligned} \tag{A3}$$

The first term on the right-hand side of (A3) contributes a linear pressure field that balances the force imparted to the fluid by the point forces to satisfy the force balance over each periodic cell. The associated Green's function tensor for the stress, adapted from expressions (2.22) of van de Vorst [9], is

$$\begin{aligned} T_{ijl}(\mathbf{x}, \mathbf{x}_0) = \; & -\delta_{il}\frac{4\pi}{A_c}\,(x_j - x_{0_j}) \\ & + 2\xi^2 \sum_n \exp(-\hat{r}_n^2)\Bigg[\delta_{jl}(x_i - x_{n_i}) + \delta_{ij}(x_l - x_{n_l}) \\ & - 2\left(1 + \frac{1}{\hat{r}_n^2}\right)\frac{(x_i - x_{n_i})(x_j - x_{n_j})(x_l - x_{n_l})}{r_n^2}\Bigg] \\ & + \frac{4\pi}{A_c}\sum_m \Bigg[\frac{1}{|\mathbf{k}_m|}\left(1 + \frac{\hat{k}_m^2}{4}\right)\left(2\frac{\mathbf{k}_{m_i}\mathbf{k}_{m_j}\mathbf{k}_{m_l}}{|\mathbf{k}_m|^3} - \frac{\delta_{ij}\mathbf{k}_{m_l} + \delta_{lj}\mathbf{k}_{m_i}}{|\mathbf{k}_m|}\right) \\ & - \delta_{il}\frac{\mathbf{k}_{m_l}}{|\mathbf{k}_m|}\Bigg]\sin[\mathbf{k}_m \cdot (\mathbf{x} - \mathbf{x}_0)]\exp\left(-\frac{\hat{k}_m^2}{4}\right). \end{aligned} \tag{A4}$$

The first term on the right-hand side incorporates the linear variation of the normal stresses due to the pressure.

References

1. T. G. Mason, J. Bibette, and D. A. Weitz, Yielding and flow of monodisperse emulsions. *J. Colloid Interf. Sci.* 179 (1996) 439–448.
2. X. Li and C. Pozrikidis, The effect of surfactants on drop deformation and on the rheology of dilute emulsions in Stokes flow. *J. Fluid Mech.* 341 (1997) 165–194.

3. S. Yon and C. Pozrikidis, A finite-volume / boundary-element method for flow past interfaces in the presence of surfactants, with application to shear flow past a viscous drop. *Computers & Fluids* 27 (1998) 879–902.
4. D. A. Reinelt and A. M. Kraynik, Simple shearing flow of dry soap foams with tetrahedrally closed-packed structure. *J. Rheol*. 44 (2000) 453–471.
5. A. Johnson and A. Borhan, Effect of insoluble surfactants on the pressure-driven motion of a drop in a tube in the limit of high surface coverage. *J. Colloid Interf. Sci.* 218 (1999) 184–200.
6. C. Pozrikidis, Interfacial dynamics for Stokes flow. *J. Comp. Phys.* (2001) in press.
7. H. Aref and D. L. Vainchtein, The equation of state of a foam. *Phys. Fluids* 12 (2000) 1070–6631.
8. C. Pozrikidis, *Boundary Integral and Singularity Methods for Linearized Viscous Flow.* Cambridge: Cambridge University Press (1992) 259 pp.
9. G. A. L. van de Vorst, Integral formulation to simulate the viscous sintering of a two-dimensional lattice of periodic unit cells. *J. Eng. Math.* 30 (1996) 97–118.
10. S. R. Breit, The potential of a Rankine source between parallel planes and in a rectangular cylinder. *J. Eng. Math.* 25 (1991) 151–163.
11. X. Li, H. Zhou, and C. Pozrikidis, A numerical study of the shearing motion of emulsions and foams. *J. Fluid Mech.* 286 (1995) 379–404.
12. C. Pozrikidis, Computation of periodic Green's functions of Stokes flow. *J. Eng. Math.* 30 (1996) 79–96.
13. S. K. Lucas, R.Sipcic, and H. A. Stone, An integral equation solution for the steady-state current at a periodic array of surface microelectrodes. *SIAM J. Appl. Math.* 57 (1997) 1615–1638.
14. C. Pozrikidis, Conductive mass transport from a semi-infinite lattice of particles. *Int. J. Heat Mass Transfer* 43 (2000) 493–504.
15. C. Pozrikidis, Theoretical and computational aspects of the motion of three-dimensional vortex sheets. *J. Fluid Mech.* 425 (2000) 335–366.
16. M. M. Fyrillas and C. Pozrikidis, Conductive heat transport across rough surfaces and interfaces. *Int. J. Heat Mass Transfer* (2001) in press.
17. C. Pozrikidis, Shear flow over a particular or fibrous plate. *J. Eng. Math.* 39 (2001) 3–24.
18. M. R. Kennedy, C. Pozrikidis, and R. Skalak, Motion and deformation of liquid drops, and the rheology of dilute emulsions in simple shear flow. *Computers and Fluids* 23 (1994) 251–278.
19. X. Li, R. Charles, and C. Pozrikidis, Simple shear flow of suspensions of liquid drops. *J. Fluid Mech.* 320 (1996) 395–416.
20. R. Charles and C. Pozrikidis, Effect of the dispersed phase viscosity on the simple shear flow of suspensions of liquid drops. *J. Fluid Mech.* 365 (1998) 205–233.